SQU Journal for Science, 2023, 28(2), 28-43 DOI:10.53539/squjs.vol28iss2pp28-43
Sultan Qaboos University

Preparation and Characterization of Iron Oxide Nano-adsorbent by Enteromorpha Flexuosa Algae obtained from Yanbu Red Sea, Saudi Arabia

Alaa Elmi[1], Rafat Afifi Khattab[2], Omar M.L. Alharbi[3], Gunel Imanova[4] and Imran Ali*[1,5]

[1]Department of Chemistry, School of Sciences, Taibah University, Medina 41477, Saudi Arabia, [2]Marine Science Department, Suez Canal University, Ismailia 41522, Egypt [3]Department of Biology, School of Sciences, Taibah University, Medina 41477, Saudi Arabia[1], [4]Institute of Radiation Problems, Ministry of Science and Education Republic of Azerbaijan, Baku AZ-1143, Azerbaijan, [5]Department of Chemistry, Jamia Millia Islamia, New Delhi 110025, India. *Email: drimran.chiral@gmail.com.

ABSTRACT: Water contamination caused by toxic cadmium metal ions is a worldwide problem. There is a need to explore new methods of cadmium removal from water. The green algae *Enteromorpha flexuosa*, obtained from the Red Sea in Yanbu, Saudi Arabia, was used to prepare iron nanoparticles. TEM, FT-IR, XRD, and SEM techniques were used to characterize the prepared nanoparticles. The prepared nanoparticle's surface was rough, with nanoparticle sizes ranging from 10 to 50 nm. The developed nanoparticles were used to adsorb cadmium ions from water in batch mode. With a 25.0 µg/L concentration, a temperature of 25˚C, 7.0 pH, 60 minutes contact time and 0.5 g/L dose, the maximum removal of cadmium was 48.2 µg/g. The sorption efficiency was measured using the Dubinin-Radushkevich, Temkin, Langmuir and Freundlich models. The amounts of ΔG° were -8.0, -9.93 and -12.24 kJ/mol while the values of ΔS° and ΔH° were -30.96 x 10^{-3} kJ/mol and 37.79 x 10^{-2} kJ/mol. These data confirmed the endothermic nature of cadmium metal ions removal. Along with the liquid film diffusion process, the adsorption adopted the kinetics of pseudo-second-order type. The recorded adsorption method is fast, cost-effective, and environmentally friendly and can be applied for testing the elimination of cadmium metal ions in natural waters.

Keywords: Green synthesis; Nanoparticles; Adsorption; Water treatment; Modeling; Kinetics and thermodynamics.

تحضير وتوصيف الممتز النانوي لأكسيد الحديد بواسطة طحلب *Enteromorpha Flexuosa* المستخرج من ينبع البحر الأحمر، المملكة العربية السعودية

علاء علمي، رأفت عفيفي خطاب، عمر محمد الحربي، جونيل إيمانوفا و*عمران علي

الملخص: يعد تلوث المياه بسبب أيونات معدن الكادميوم السامة مشكلة عالمية، ولا تزال هناك حاجة لإستكشاف طرق جديدة لإزالة الكادميوم من الماء. تم إستخدام الطحالب الخضراء Enteromorpha flexuosa، التي تم الحصول عليها من البحر الأحمر في ينبع بالمملكة العربية السعودية، لتحضير جزيئات الحديد النانوية. تم إستخدام تقنيات TEM، FT-IR، XRD، وSEM لتوصيف الجسيمات النانوية المحضرة. كان سطح الجسيمات النانوية المحضرة خشنًا، وتتراوح أحجام الجسيمات النانوية من 10 إلى 50 نانومتر. تم إستخدام الجسيمات النانوية المطورة لإمتصاص أيونات معدن الكادميوم من الماء في وضع الدفعة. مع تركيز 25.0 ميكروغرام/لتر، ودرجة حرارة 25 درجة مئوية، ودرجة حموضة 7.0 ، ووقت تلامس 60 دقيقة وجرعة 0.5 غرام/لتر، كان الحد الأقصى لإزالة الكادميوم 48.2 ميكروغرام/لتر. تم قياس كفاءة الإمتصاص بإستخدام نماذج Dubinin-Radushkevich وTemkin وLangmuir وFreundlich. كانت كمية ΔG°، 8.0-9.93- و-12.24 كيلو جول/مول بينما كانت قيم ΔS° و ΔH° و10^{-3} × 30.96- كيلو جول/مول و37.79 × 10^{-2} كيلو جول/مول. أكدت هذه البيانات الطبيعة الماصة للحرارة لإزالة أيونات معدن الكادميوم. جنباً إلى جنب مع عملية إنتشار الغشاء السائل، إعتمدت عملية الإمتزاز حركية النوع من الدرجة الثانية الزائفة. تتميز طريقة الإمتزاز المسجلة بأنها سريعة وفعالة من حيث التكلفة وصديقة للبيئة ويمكن تطبيقها لإختبار التخلص من أيونات معدن الكادميوم في المياه الطبيعية.

الكلمات المفتاحية: التخليق الأخضر؛ الجسيمات النانوية؛ الإمتزاز؛ معالجة المياه؛ النمذجة؛ الحركية والديناميكا الحرارية.

1. Introduction

Throughout the last few decades, water safety has been a big concern. [1-7]. Toxic trace metal ions are among the numerous water contaminants that are extremely harmful due to their serious toxicity and side effects, which include cancer [8]. These ions have tendency for interacting with proteins and enzymes and are not biodegradable [9-11]. These metal ions appear to accumulate in tissues, causing a variety of diseases and health problems. Humans are thought to be at risk from exposure to these metals, even at trace levels [12-15]. As a result, scientists, academics, and government officials are all concerned about metal contamination. Nanotechnology's goals are to develop eco-friendly designs in order to reduce health and environmental risks by finding ways to substitute current applications with green nanotechnology products. Nanotechnology is the production of components in particular by a number of material processes and/or ingredients, ultimately to be applied in a range of applications [17]. A nanoparticle is well-defined as a minute element with a minimum of at least one dimension in the range of 10 to 100 nm. They have unique electrochemical, thermal, and optical properties making them useful in numerous applications in the areas of energy, environment, medicine, chemistry, agriculture, communication, information, consumer goods, and heavy industry.

To remove toxic metal ions from aqueous media, some researchers have used nanoparticles as adsorbents. Because of their catalytic strength, small size, large number of active sites, high reactivity, and ease of separation for interacting with various contaminants, nanomaterials make excellent adsorbents. These features are related to the great adsorption capabilities, as determined by the adsorption power. Zhang [18] investigated the characterization, synthesis, and use of Fe^o/Ni^o, Fe^o/Ag^o, Fe^o/Pt^o, Fe^o/Co^o and Fe^o/Pd^o nanoscale Fe^o particles, as well as Fe^o/Co^o Fe^o/Ni^o, Fe^o/Ag^o and Fe^o/Pt^o nanoscale Fe^o particles. Cr(VI) was efficiently reduced to mobile and less toxic Cr(III) type using Fe° and bimetallic Fe^o nanoparticles. Deliyanni and Matis [19] extracted cadmium using akaganeite (-FeOOH) nanoparticles with a 17.1 mg/g adsorption potential. Furthermore, since the adsorption potential increased from 30% to 90% as the temperature rises from 25 to 65 ºC; the whole process was exothermic. In order to remove Cr(VI) from groundwater, it was discovered that starch-stabilized Fe° nanoparticles were more adsorbent than native zero-valent metal particles. As pH and dosage were increased, adsorption ability was found to decrease. Lazaridis, *et al.* [20] synthesized nanocrystalline akageneite rod-like nanoparticles (3-6 nm diameter) with a comprehensive removal rate of 80.0 mg/g to extract Cr(VI). According to Hu, *et al.* [21] Cr(VI) elimination from wastewater using maghemite nanoparticles was 19.2 mg/g. The nanoparticles had an established diameter of 10 nm, and the maximum adsorption occurred within 15 minutes at pH 2.5. Di, *et al.* [22] used carbon nanotubes to strip Cr(VI) from drinking water. The strongest Cr(VI) adsorption, according to the researchers, occurred at a pH range of 3.0-7.4, with a power of 30.2 mg g^{-1}. The use of chitosan-Fe(0) nanoparticles to purify water from Cr(VI) was recorded by Geng, *et al.* [23].

Recently, scientists started to prepare nanoparticles using plant extracts. This is a green and environmentally friendly process. Some reviews have been presented on the synthesis of various nanoparticles using the green approach [24-26]. Only a few authors exploited these nanoparticles for water treatment. Ehrampoush, *et al.* [27] used the extract of tangerine peel and prepared nanoparticles of iron oxides for the decontamination of cadmium in water. Biosynthesis of stable iron nanoparticles was carried out using Phoenix dactylifera L. extract which was able to reduce iron ions to iron nanoparticles [28]. Iron oxide nanoparticles (IONPs) were synthesized using a cost-effective and eco-friendly method, taking *Moringa oleifera* leaves extract as a bio-reducer [29]. The influence of different parameters on removal efficiency, such as metal concentration, adsorbent dosage, pH and contact time was studied. Ehrampoush, *et al.* [30] prepared iron oxide nanoparticles by green synthesis for the removal of cadmium from aqueous solution. The authors used plant extract to make nanoparticles. Zhu, *et al.* [31] synthesized nanoscale zero-valent iron/Cu prepared by green synthesis. The exclusion effectiveness of Cr (VI) was 94.7 percent at a pH of 5 and a temperature of 303 K with observable rate constant K_{obs} values of 0.07430, 0.09650, 0.1183, and 0.1473 min1 at 298, 303, 308, and 313 K. Ali and co-workers prepared complex and functionalized iron nano particles using a black tea extract. The nanoparticles were used for the removal of azorubine dye [32], tetracycline and chlortetracycline antibiotics [33], actinides and rare earth elements [34], dioxidine [35], samarium ions [36], ketoprofen [37], and tetracycline antibiotics [38]. The authors tested their data with various models. The removal of these pollutants was in the range of 80-90 %. The objectives of this study are to prepare a new generation nano-adsorbent by green methods as well as the removal of cadmium using batch mode.

2. Experimental

2.1 Materials

The chemicals were purchased from Merck, Darmstadt, Germany, included cadmium nitrate, iron chloride, iron sulphate, sodium hydroxide, hydrochloric acid, and others. Purified water was obtained by using Heal Force water purification system, China. The pH of the solutions was evaluated using a Control Dynamics pH meter (Model APX175 E/C). The nanoparticles were removed by a powerful magnet. FT-IR Nicolet380 was used to record FT-IR spectra. Powdered X-ray diffraction was conducted on a Philips PX-1830 diffractometer with a proportional counter detector, a Cu filter on secondary optics, 30 mA current, Cu-K_α radiation (λ = 1.54 nm), and 25 kV voltage. Images

were captured using scanning electron and transmission microscopes. ICP-MS Agilent Technologies 7500 Series was used to assess the residual content of Cd(II), as per the normal procedure.

2.2 Iron nanoparticle preparation

Preparation of iron nanoparticles (NPs) using Green technology was done using a standardized protocol [39,40]. The Red Sea alga (*Enteromorpha flexuosa*, 10.0 g/L) was rinsed numerous times using deionized water before being blended for 30 minutes with 500 mL of deionized water. The paste was heated at 80 ºC for about 2-3 hrs. It was then cooled before being filtered through Whatman filter paper (No. 24). The solutions of $FeCl_3$ and $FeSO_4$ (0.1 M) were prepared in 250 and 125 mL, separately and respectively. Both solutions were mixed together. Now, 500 ml extract of alga was mixed slowly with constant string. 0.1 N sodium hydroxide was used to keep the pH of the solution at 10. For 24 hours, the solution was stirred. A strong magnet was used to isolate the settled nanoparticles. The nanoparticles were splashed with deionized water numerous times before being immersed in 70% ethanol. The nanoparticles were dried at 100 °C in an oven for 5 hrs. These were cooled and prepared for later use in a vacuum desiccator. The green approach to the synthesis of iron oxide nanoparticles is depicted schematically in Figure 1.

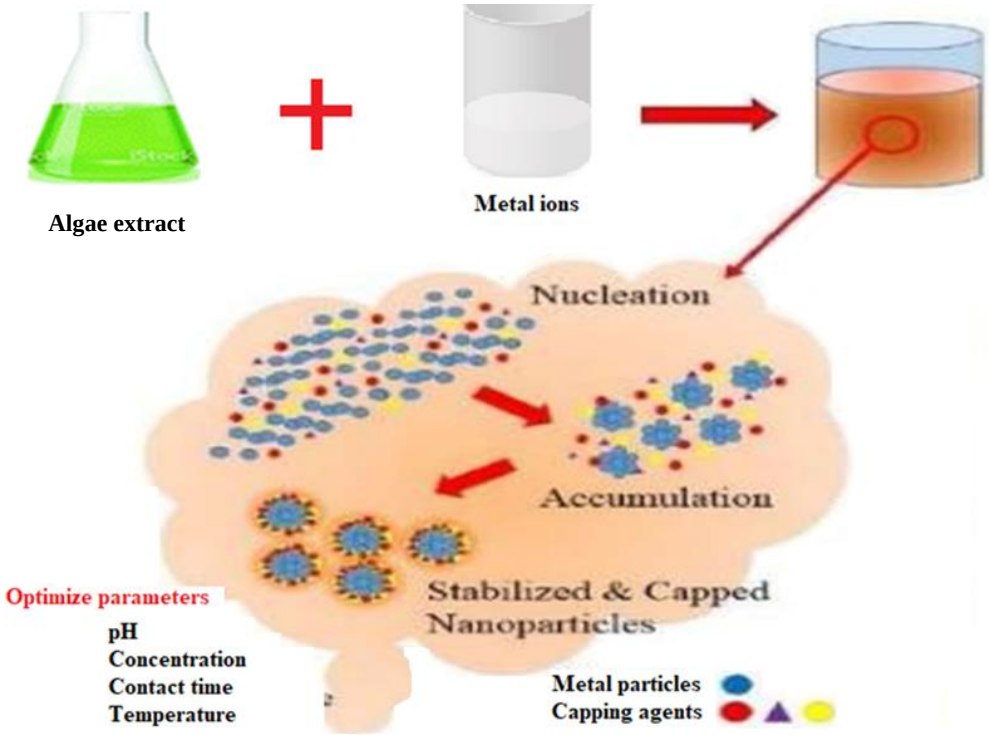

Figure 1. The green method used to synthesize iron nanoparticles.

2.3 Characterization of iron nanoparticles

The synthesized iron nanoparticles were classified using FT-IR, XRD, TEM and SEM approaches. At a voltage of 10 kV, photographs of samples were taken at various magnifications. Using a Philips PX-1830 diffractometer, Cu-K_α radiation (λ = 1.54 nm) was used to obtain X-ray diffraction (XRD) patterns of native and iron nano-impregnated particles using a proportional counter detector, a secondary optics Cu filter, 25 kV voltage and 30 mA current. At a rate of 3 °C per minute, the temperature from 10 to 80 °C for the iron nano-impregnated particles were scanned.

2.4 Adsorption studies

All of the adsorption tests were performed in a thermostatic water bath shaker at a specific temperature and duration. Following adsorption, the liquid and solid materials were separated using centrifugation. The concentrations of Cd(II) in solution samples were measured using an ICP-MS system. Adsorption isotherms were investigated using a concentration range of 5-30 µg/L, a pH range of 2-9.0, a contact time of 10-90 minutes, a dosage of 0.1-0.50 g/L, and temperatures of 15-35 °C. Isothermal and kinetic parameters were determined using various mathematical simulations. Data from batch studies were used to measure the equilibrium Cd(II) uptake potential. It was calculated using the equation below.

$Q_e = (C_0-C_e)/m.$

3. Results and Discussion

3.1 Iron nanoparticles characterization

Changes in the color of algae extract were used to assess the development of iron nanoparticles. The green color of the algae extracts changed from brown to black after mixing in iron salt solution. The color change is an indication of the chemical reaction and formation of nanoparticles. The physical appearance of iron oxide nanoparticles is shown in Figure 2. The FT-IR spectra of nanoparticles showed peaks at 574 cm^{-1} indicating the presence of Fe-O. A Bruker D8 fitted with monochromatic copper radiation (K_α, λ = 0.154 nm) was used to record the nanoparticles' X-ray diffraction (XRD) pattern at room temperature. XRD patterns of Fe_3O_4 NPs confirmed the formation of a pure phase of Fe_3O_4 NPs. The peaks were obtained at the 2θ of 30, 40, 60, and 70 indicating the presence of iron oxide, iron(III) oxide-hydroxide, and free Fe^0 (zero-valent iron), respectively. The XRD pattern indicates the amorphous nature of nanoparticles. A TOPCON 002B transmission electron microscope (TEM) with a GATAN GIF 200 electron imaging filter and a 200 kV operating voltage (point resolution 0.18 nm) was used to study the morphology and crystalline structure of the nanoparticles. Figures 3 and 4 display SEM and TEM images of the prepared nanoparticles, respectively. An evaluation of SEM images indicates the rough and crystalline surface. The evaluation of TEM images shows nanoparticle sizes ranging from 10 to 50 nm.

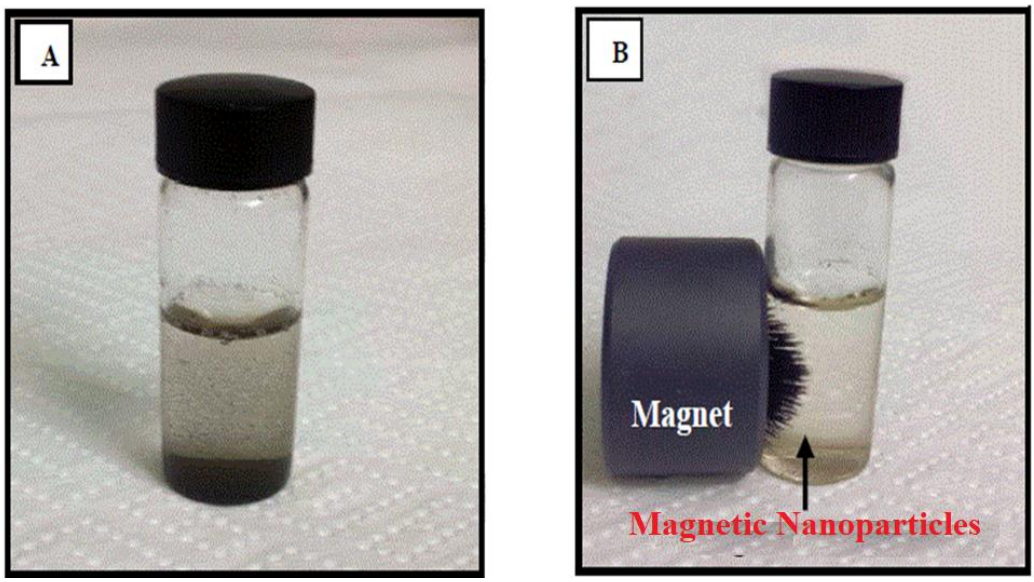

Figure 2. Iron oxide magnetic nanoparticle (A): before and (B): after magnetic property.

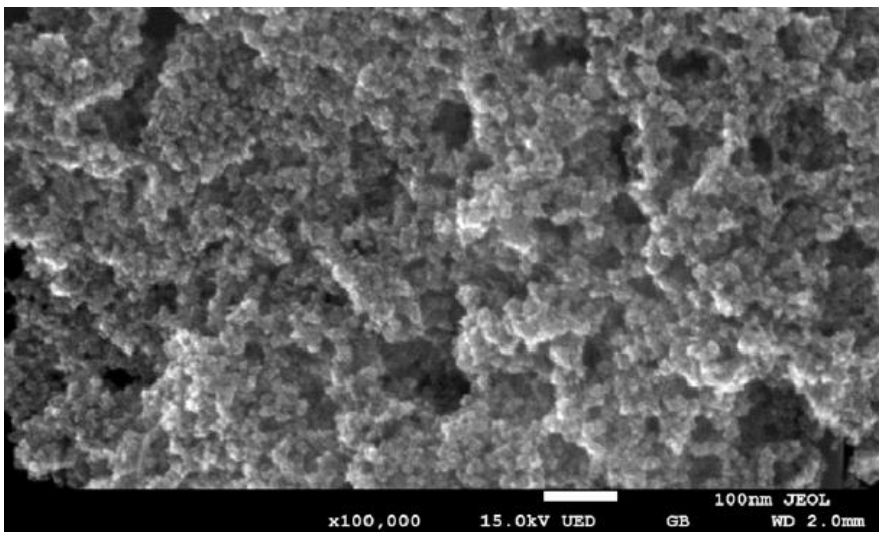

Figure 3. SEM of iron nanoparticles.

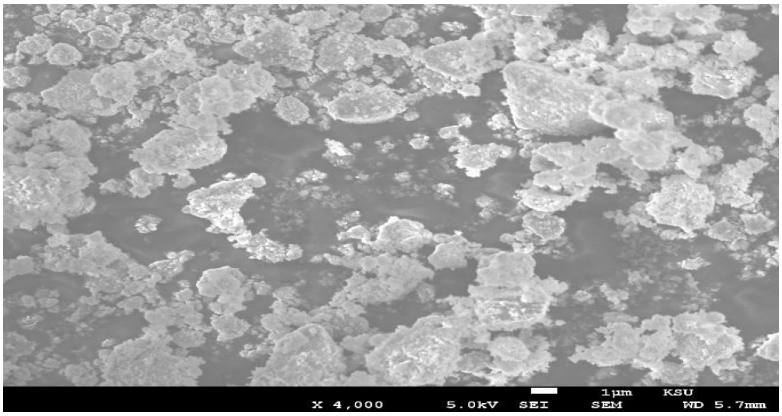

(a)

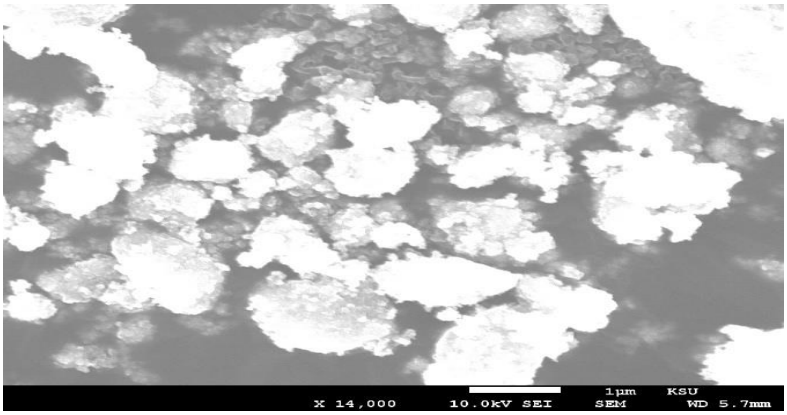

(b)

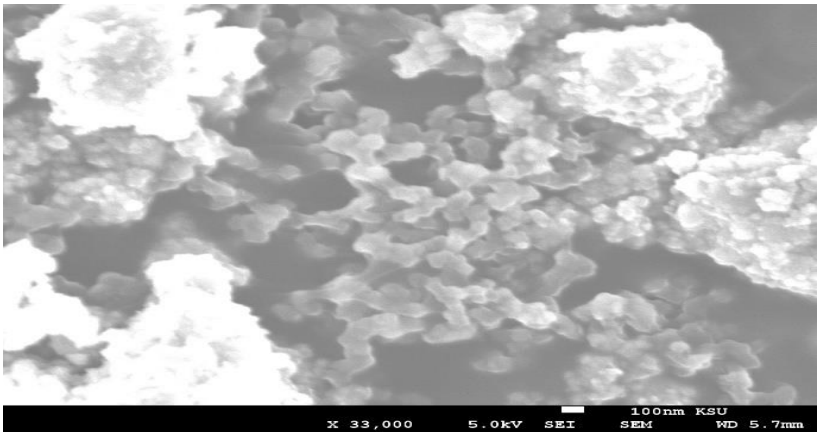

(c)

Figure 4. TEM images of iron nanoparticles at different magnifications, (a): 4,000, (b): 14,000 and (c): 33,000.

3.2 Adsorption studies

3.2.1 Effect of concentration

The concentration was optimized by varying the concentration between 5 and 30 g/L. The temperature was 25°C, the pH was 7.0, the dose was 0.5 g/L, and the contact time was 25 minutes. As previously mentioned, the residual concentration of Cd(II) was determined. Figure 5 depicts this effect, with the maximum uptake of Cd(II) at 25.0 g/L. Adsorption increased rapidly from 9.5 µg/g at 5.0 g/L to 48.2 µg/g at 25.0 g/L concentration (as seen in this graph. After a concentration of 25.0 g/L, the adsorption became constant. At higher concentrations, adsorption capacities did not increase. As a result, the optimum concentration was determined to be 25.0 g/L.

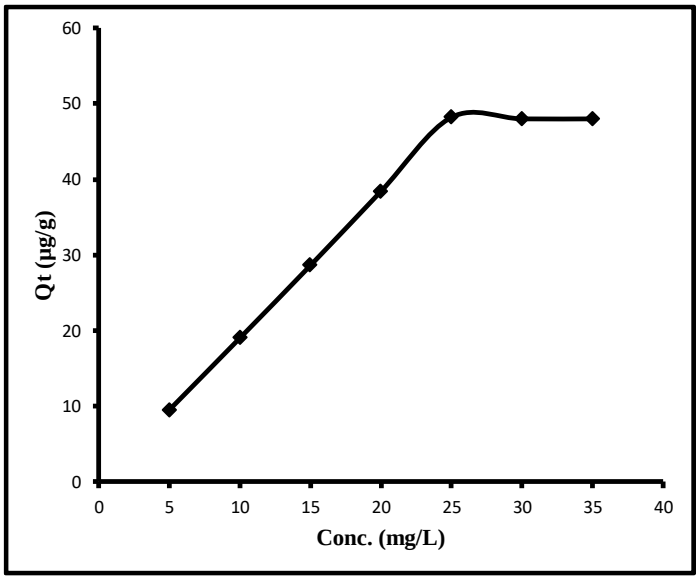

Figure 5. The initial concentration effect on cadmium removal.

3.2.2 Effect of contact time:

Experiments ranging from 10 to 90 minutes were used to maximize the impact of contact time. Contact time was tested against the other variables of 25 g/L concentration, pH 7.0, dosage 0.5 g/L, and temperature 25 °C. Figure 6 depicts the outcome of this effect. The adsorption capacities increased from 10 (43.0 g/g) to 60 minutes (48.0 g/g) as seen in this graph. More contact time did not improve adsorption. Therefore, it was concluded that 60 minutes was the optimized time.

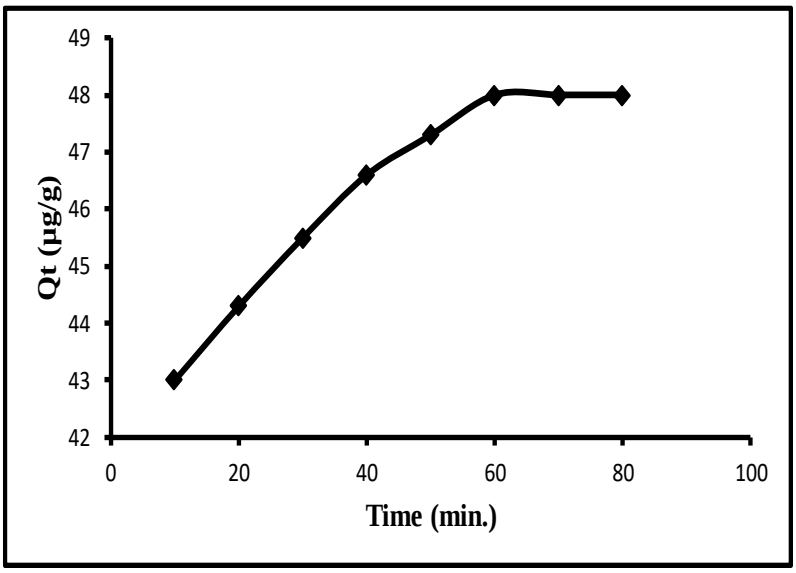

Figure 6. The contact time effect on cadmium removal.

3.2.3 Effect of pH

Experiments at various pHs were used to maximize the pH of adsorption (2-9). Contact time was 60 minutes, concentration was 25 g/L, the dosage was 0.5 g/L, and the temperature was 25 °C. Figure 7 depicts the outcome of this effect. The adsorption capacities increased from 4.5 µg/g at pH 2.0 to 48.5 µg/g at pH 7.0 as seen in this graph. More adsorption would be difficult to accomplish with a higher pH. As a result, it was concluded that pH 7.0 was the best.

3.2.4 Effect of dosage

The effect was investigated using a dosage range of 0.1-0.8 g/L. Contact time was 60 minutes, concentration was 25 g/L, pH was 7.0, and the temperature was 25 °C. Figure 8 depicts the outcome of this effect. The adsorption

capacities increased from 4.28 µg/g at 0.1 g/L dose to 48.0 µg/g at 0.5 g/.L dose as seen in this graph. Higher dosage did not improve adsorption. As a result, the 0.5 g/L dose was determined to be the best.

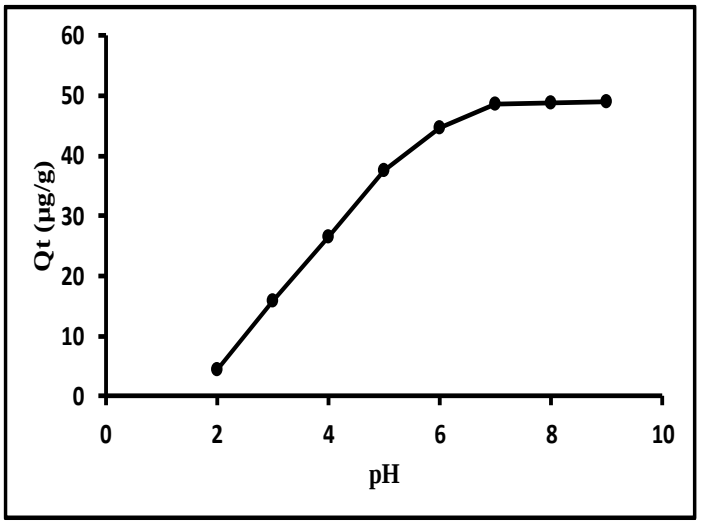

Figure 7. pH effect on cadmium removal.

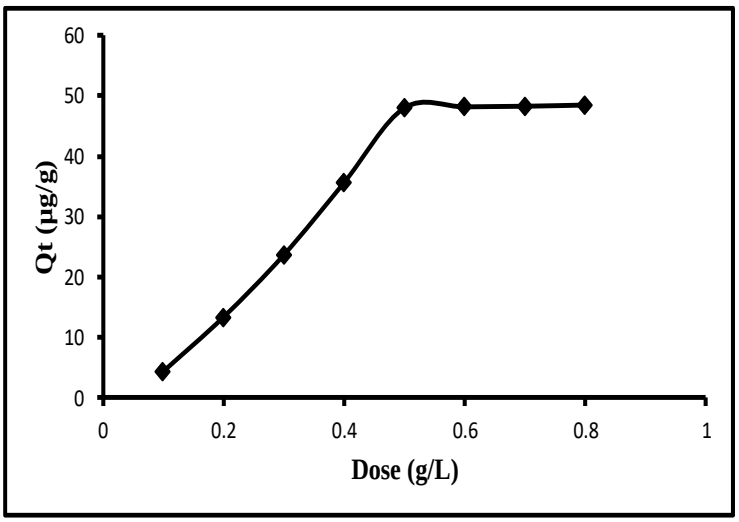

Figure 8: Effect of dose on cadmium removal.

3.2.5 Effect of temperature

Temperature effects on adsorption were investigated at 15, 25, and 35°C. Contact time was 60 minutes, concentration was 25 µg/L, pH was 7.0, and the dosage was 0.5 g/L. Figure 9 depicts the results of this parameter. The sorption of Cd(II) decreased as the temperature increased, suggesting an exothermic adsorption process. The order of Cd(II) removal was 15 > 25 > 35 °C. Of course, since most water sources have a temperature range of 15-35 °C, the adsorption process was deemed environmentally friendly. All the experiments were carried out 3 times (n = 3) and the standard deviation ranged from 0.45 to 0.67%.

3.3 Adsorption models

Well-known models illustrate the elimination of the cadmium metal ion. These are listed in more detail below.

3.3.1 Langmuir model

The most commonly used method for measuring the amount of adsorbate on an adsorbent as a function of a given temperature at partial pressure or concentration is the Langmuir adsorption model. It reflects a molecule's adsorption on an idealized surface. The molecule is thought to bind to several different locations on the solid's surface.

In the most basic case this model makes the following assumptions: the adsorption of a single adsorbate onto several identical sites on the surface of a solid

1. There are no corrugations on the surface containing the adsorbing sites (assuming the surface is homogeneous).
2. The adsorbing gas becomes immobile as a result of the adsorption process.

3. Every location is the same.
4. Each molecule can only be stored in one site at a time (mono-layer coverage only).
5. Adsorbate molecules on neighboring sites have no interactions with one another.

With mono-layer sorption, the secret to the Langmuir model is the assumption of even sorption energy on the adsorbent surface. Equation 1 is the model's linear form. [41].

$$\frac{1}{q_e} = \frac{1}{q_0} + \frac{1}{q_0 b C_e} \quad (1)$$

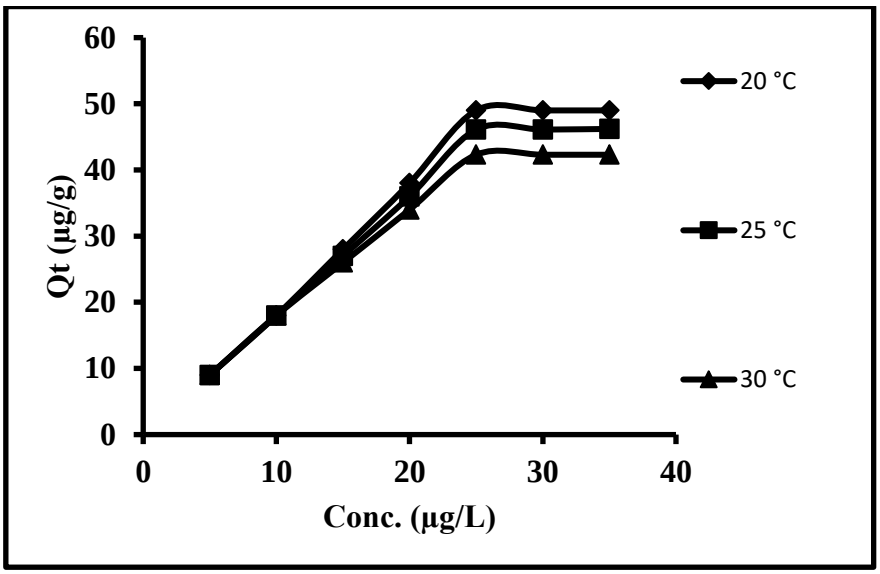

Figure 9. Effect of temperature on the removal of cadmium.

Table 1. Models parameter values for cadmium metal ion.

Models	Parameters	Numerical Values		
		15 ºC	25 ºC	35 ºC
Langmuir	Q_0 (µg/g)	28.99	54.95	119.05
	b (L/µg)	0.80	0.51	0.27
	R_L	0.61	0.69	0.80
	R^2	0.980	0.992	0.947
Freundlich	k_F (µg/g)	76.95	54.29	44.72
	n (µg/L)	0.50	0.64	0.77
	R^2	0.995	0.978	0.899
Temkin	K_T (L/µg)	1.58	1.59	1.64
	B_T (kJ/mol)	0.018	0.023	0.029
	R^2	0.996	0.927	0.807
Dubinin-Radushkevich	Q_e (µg/g)	213.80	157.32	123.87
	E (kJ/mol)	0.78	0.83	0.88
	R^2	0.948	0.954	0.916

A straight line is obtained when 1/qt is plotted against 1/Ce (Figure 10), demonstrating the Langmuir model's usefulness. The intercept and slope of the graphs determine the values of the constants (b and Q_0) (Table 1). For Cd(II), the values of q_0 and b ranged from 28.99 to 119.05 g/g. RL values ranged between 0.61 and 0.80. At all temperatures, the regression constants' magnitudes ranged from 0.947 to 0.992. This is where the model's applicability is proven.

3.3.2 Freundlich model

For rough surfaces, the most powerful multisite adsorption isotherm is the Freundlich isotherm. Freundlich isotherm adsorption, as opposed to monolayer adsorption, is multilayer adsorption on a heterogeneous surface with a non-uniform distribution of adsorption heat and affinities. The total number of adsorbates adsorbed on the adsorbent's surface is called the total number of all sites. As the adsorption process continues, the adsorption energies decrease exponentially. This is how the Freundlich adsorption isotherm is calculated:

$$\log Q_e = \log k_F + \frac{1}{n}\log C_e \quad (2)$$

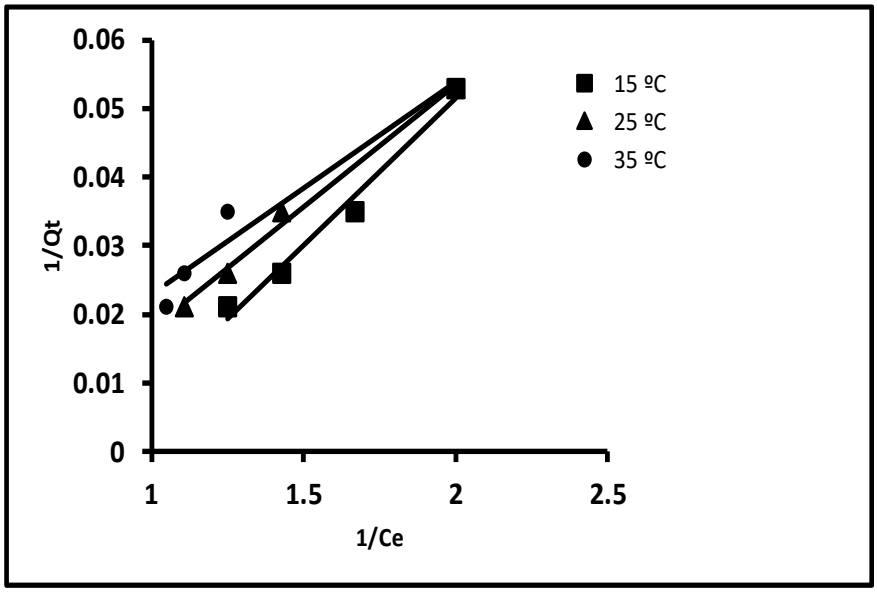

Figure 10. Langmuir plots showing cadmium adsorption.

Freundlich constants, Kf (µg/g) and n (µg/L) are empirical constants. The exponent is denoted by n, and the relative adsorption potential of the adsorbent is denoted by k_F. (1-10 for a successful adsorption process). The plot of logQt vs logCe should be a straight line, and the intercept on the logQt-axis should give the value of $logk_F$, according to equation 2. (Figure 11). The adsorption strength is determined by the slope (equal to 1/n). The lower the 1/n value, the more heterogeneous the adsorption process. Chemisorption was suggested by 1/n values less than unity. Above unity values, on the other hand, indicate cooperative adsorption, which is characterized by intense interactions between adsorbate molecules on the adsorbent's surface. At three temperatures, the values of K_F for Cd(II) ranged from 44.72 to 76.95. (Table 1). KF values increased, indicating an improvement in sorption capacity on the adsorbent and a boost in sorption efficiency. At different temperatures, the values of n for Cd(II) ranged from 0.899 to 0.995 1.79, indicating that the adsorbent has a desirable sorption. The model's applicability was verified at this point.

3.3.3 Temkin model

This model accounts for the adsorbate's indirect interactions with the adsorbent on the adsorbent surface. Temkin discovered that the heat of adsorption begins to decrease as the amount of coverage increases. It can be determined using the equation below [42].

$$q_e = \left(\frac{RT}{B_T}\right)\ln K_T + \left(\frac{RT}{B_T}\right)\ln C_e \quad (3)$$

The equilibrium binding constant and sorption heat are expressed by the constants KT and BT, respectively. As Qt is plotted against log Ce (Figure 12), the intercept and slope correspond to the constants KT and BT. Table 1 summarizes the BT and KT values that were predicted. Cd(II) had BT values ranged from 0.018 to 0.029 kJ/mol. The modified BT values revealed a loose interface between the adsorbent and the Cd(II). As a result, it was believed that adsorption occurred via an ion exchange process. The KT values for Cd(II) ranged from 1.58 to 1.64 L/µg. These results indicated that Cd(II) was well bound to the adsorbent.

3.3.4 Dubinin-Kaganer-Radushkevich (DKR) model

The key to the Dubinin-Radushkevich model is the presumption of different physical and chemical adsorption rates. This model also explains a Gaussian energy delivery on an irregular surface [43]. The linear forms of the model are Equations 4 and 5.

$$\ln q_e = \ln q_m - \beta\varepsilon^2 \quad (4)$$

$$\varepsilon = RT\ln\left(1 + \frac{1}{C_e}\right)$$

The [saturation ability ($mol^2\ J^{-2}$)] is used to evaluate the likelihood of sorption through a physical or chemical process. Equation 7 is used to measure [Polanyi potential ($\mu g\ g^{-1}$)]. [44].

$$\varepsilon = 1/\sqrt{\beta} \quad (5)$$

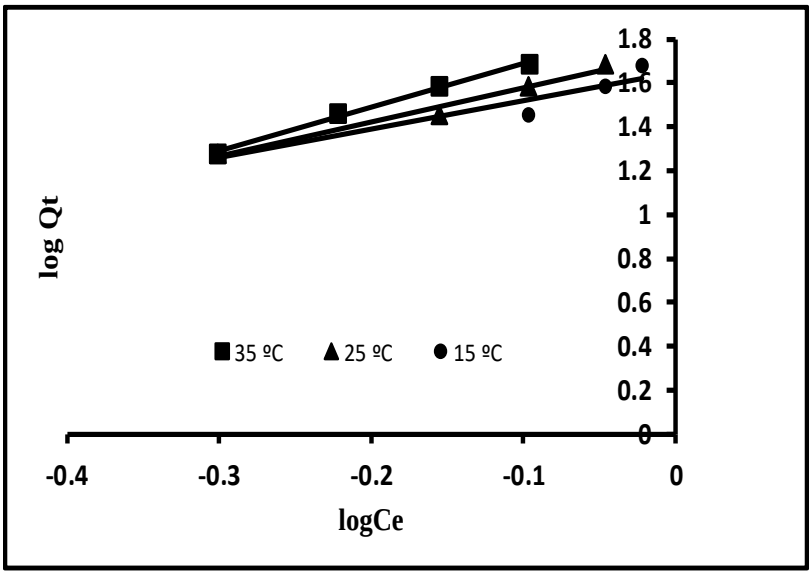

Figure 11. Freundlich plots showing cadmium adsorption.

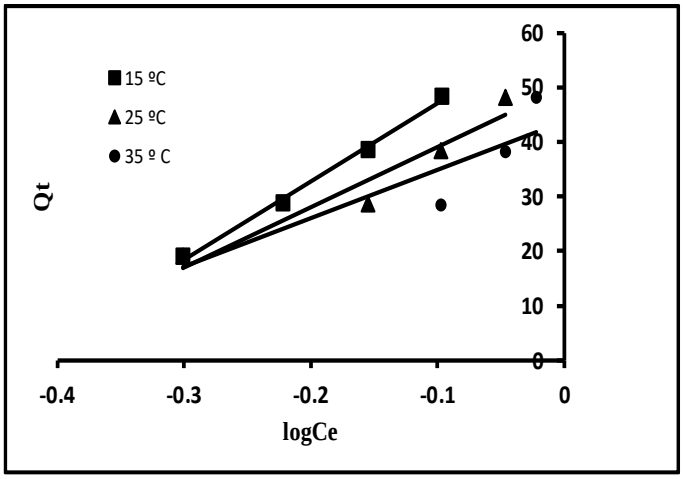

Figure 12. Temkin plots showing cadmium adsorption.

A straight line is formed when lnQt is plotted against E2 (Figure 13), with intercept and slope corresponding to ε and qe, respectively. Table 1 shows the values of qe for the average sorption free energy per mole of Cd. These qe and kJ/mol values ranged from 123.87 to 213.8 µg/g and 078 and 0.88 kJ/mol, respectively. Positive and lower values than 8.0 KJ/mol confirm ion exchange and physical sorption of Cd(II) onto the sorbate. Lower BT values in the Temkin segment confirm these scenarios.

3.4 Thermodynamics study

The thermodynamic process is defined by energy, enthalpy, and entropy. As shown below, Vant Hoff's equation connects the equilibrium constant to the Gibbs free energy transition of adsorption.

$$\Delta G^\circ = -RT \ln K \quad (6)$$

ΔG°, T, R, and K stand for free energy change (kJ/mol), absolute temperature (K), uniform gas constant (0.008314 kJ mol-1 K-1), and equilibrium constant, respectively. When K is replaced with Xm, the equation becomes as follows (Langmuir constant).

$$\Delta G^\circ = -RT \ln Q_0 \quad (7)$$

ΔG° values at 15, 25, and 35 °C were determined and found to be -8.0, -9.93, and -12.24 kJmol-1, respectively (Table 2). The negative ΔG° values indicate favorable and spontaneous adsorption. The following equations relate changes in entropy (S°) and enthalpy (H°) to Gibb's free energy of adsorption (ΔG°).

$$\Delta G° = \Delta H° - T\Delta S° \quad (8)$$

The following equation can be substituted for the one above.

$$\ln(Q^{o}) = \Delta S°/R - \Delta H°/RT \quad (9)$$

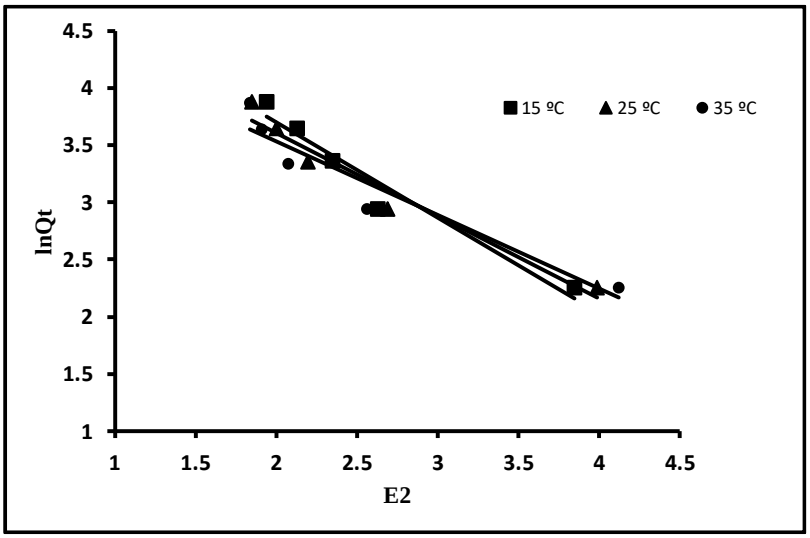

Figure 13. Dubinin-Radushkevich plots showing cadmium adsorption.

A straight line was drawn while plotting lnQo vs 1/T. (graph not shown). ΔS° was assigned to the intercept, while ΔH° was assigned to the slope. ΔH° and ΔS° had values of -37.79 x 10-2 and -30.96 x 10-3, respectively. Exothermic adsorption was demonstrated by the negative value of enthalpy shift. The entropy of the adsorption mechanism decreases as the negative value of ΔS° decreases. As a result, Cd(II) adsorption was related to a reduction in Cd mobility freedom (II).

Table 2. Values of cadmium metal ion thermodynamic parameters.

ΔG° (kJ/mol)			**ΔH° (kJ/mol)**	**ΔS° (kJ/mol K)**
T= 288 K	T=298 K	T=308 K		
-8.0	-9.93	-12.24	-37.79×10^{-2}	-30.96×10^{-3}

3.5 Modeling of Kinetics

The mechanism of adsorption was determined using kinetic simulation. It was defined by the adsorbent's and adsorbate's physical and chemical characteristics. As a result, adsorption data was used to evaluate different models. The following sub-sections go over each of these.

Table 3. Kinetic parameters for cadmium metal ion.

Kinetic models	**Kinetic parameters**	**Numerical values**
Model of pseudo-first-order kinetics	k_1 (min^{-1}) Experimental qe (μg g^{-1}) Theoretical qe (μg g^{-1}) R^2	0.421 48.2 7.94 0.978
Model of pseudo-second-order kinetics	k_2 (μg $g^{-1}min^{-1}$) Experimental qe (μg g^{-1}) Theoretical qe (μg g^{-1}) h (μg $g^{-1}min^{-1}$) R^2	0.010 48.20 49.26 10.0 0.999
Kinetic model of Elovich	α (μg $g^{-1}min^{-1}$) β (μg $g^{-1}min^{-1}$) R^2	30.20 0.022 0.999

3.5.1 Model of pseudo-first-order kinetics.

This is the first mechanism assessment model. The following equation is used to calculate it.

$$dQ_t/dt = k_1 (Q_e-Q_t) \quad (10)$$

To obtain a linearized equation, the boundary conditions of t = 0 with Qt = 0 and t = t with Qt = Qt were combined with the above equation.

$$\ln(Q_e-Q_t) = \ln_e - k_1 t \quad (11)$$

The solute number (mg/g) adsorbed at equilibrium and the equilibrium rate constant, respectively, are Qe, Qt, and k1 (min-1). Table 3 shows the results of the calculations. At a temperature of 25 °C, plotting ln(Qe-Qt) vs. t yielded the rate constant (Figure 14). With a regression coefficient of 0.978, the pseudo-first-order rate constant was 0.421 (min-1) (R2). Qe was 48.2 gg-1 in the experiment and 7.94 gg-1 in the theory, respectively. This model cannot be used since the difference between these values is 83.53 percent.
As a consequence, the pseudo-second-order kinetic model was examined.

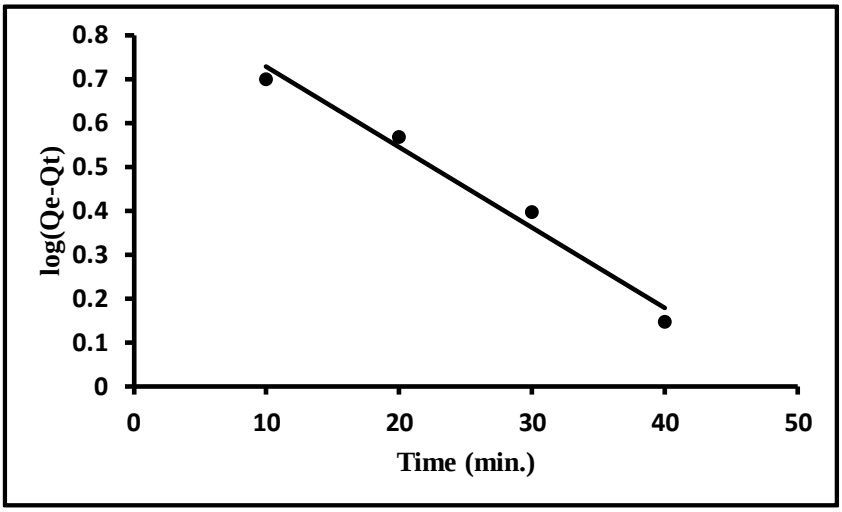

Figure 14. The adsorption elimination kinetic plot in pseudo-first order.

3.5.2 Model of pseudo-second-order kinetics

An attempt was also made to test a pseudo-second-order kinetic model using the experimental results. For the adsorption phenomenon, the following equation describes a pseudo-second-order kinetic model.

$$dQ_t/dt = k_2 (Q_e-Q_t)^2 \quad (12)$$

The definitions of Qe, Qt, and t are the same as before. With boundary conditions of t = 0 with Qt = 0 and t = t with Qt = Qt, the above equation was integrated. The equation that results is as follows:

$$t/Qt = 1/k_2Qe^2 + t/Qt \quad (13)$$

H was substituted for $k_2Q_e^2$ in the previous equation, yielding the following equation.

$$t/Q_t = 1/h + t/Q_e \quad (14)$$

where h is the adsorption rate constant at the start. It was figured out using a pseudo-second-order plot. As the time reached zero, Qt/t became hk2 is the pseudo-second-order adsorption rate constant (g/mg/min). The slope and intercept of the plot t/Qt vs t were used to measure Qe and k2 (Figure 15). Table 3 displays the measured parameters. k2 and h were 0.010 µg $g^{-1}min^{-1}$ and 10.0 µg $g^{-1}min^{-1}$, respectively. These results showed a rapid rate of adsorption at first, followed by a sluggish rate as time passed. The regression coefficient (R^2) was 0.999, suggesting that the pseudo-second-order model of the adsorption mechanism was suitable. The experimental and theoretical Qe values were 48.2 and 49.26 µg /g, respectively. It was just a difference of 2.21 %. The validity of the pseudo-second-order kinetic model was confirmed by both of these values. As a result, this model was deemed appropriate.

3.5.3 Elovich's kinetic model

Elovich's kinetic model can be used to quantify adsorption and desorption rates. Elovich's equation was created to represent the kinetics of gaseous chemo-adsorption on solid surfaces. Chien and Clayton [45] changed it after that, taking into account a linear increase in adsorption activation energy with surface coverage. The following equation describes this model.

$$dQ_t/dt = \alpha \exp(-\beta Q_t) \quad (15)$$

The initial adsorption rate is correlated by α (µg/g.min). β (µg/mg) is the desorption constant. To integrate the above equation, the boundary conditions t = 0 with Qt = 0 and t = t with Qt = Qt were used. If it is greater than one, equation 15 becomes the following.

$$Qt = \beta \ln(\alpha\beta) + \beta \ln t \quad (16)$$

The experimental findings were applied using Elovich's model. In Table 3, the values of α, β and R^2 are listed, 0.022 gmg-^{1,} and 0.999, respectively, were 30.20, mgg1min1, 0.022 gmg^{-}1, and 0.999. The adsorption rate was found to be higher than the desorption rate. Furthermore, the regression constant's value was close to one, suggesting that the model was suitable.

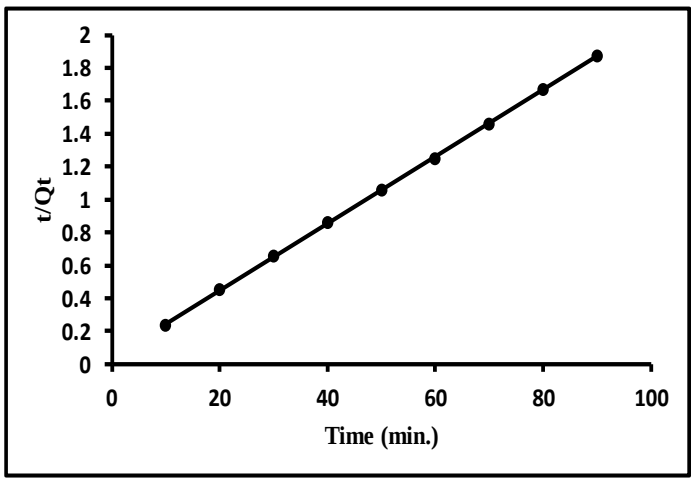

Figure 15. The adsorption removal pseudo-second-order kinetic plot.

3.6 Adsorption mechanism

Film diffusion, pore diffusion, and intra-particle diffusion are the most common pathways for adsorption. The adsorption phenomenon is controlled by the rate-determining process, which is the slowest. Intraparticle and film diffusion models were used to match the experimental results to figure out how Cd(II) sorption on the observed adsorbent works.

3.6.1 Kinetic model of intraparticle diffusion

There are several methods for adsorbate adsorption on adsorbent surfaces, including i) a liquid film is used to transport adsorbate from a bulk solution to an adsorbent surface, ii) adsorbate sorption onto an adsorbent surface, and iii) adsorbate movement within an adsorbent's pores. As a result, either surface adsorption kinetics or transport phenomena (film and intraparticle diffusions) or both control the adsorption process. The second step is very fast and cannot be used to calculate a value. The first and third measures could be used to calculate the rate. As a result, two models were used to investigate these changes. The sum of adsorbed Cd(II) and the square root of contact time may be used to measure the transfer of Cd(II) from solution to adsorption sites. The formula for this can be found below.

$$Qt = k_{ipd} t^{05} \quad (17)$$

Adsorption is caused by intra-particle diffusion (kipd) if a graph of Qt vs $t^{0.5}$ is a straight line passing through the origin and the slope of the line corresponds to the rate constant. This graph was generated by Qt vs $t^{0.5}$ (Figure not given). The rate constant was found to be 1.11 µgg^{-1}. The intercept and regression coefficients were 36.0 and 0.998. (Table 4). The graph did not move through the origin, indicating that the intra-particle diffusion model was not applicable.

3.6.2 Kinetic model of liquid film diffusion

Boyd, *et al*. [46] developed a liquid film diffusion kinetics model. The adsorption mechanism is regulated by the boundary in this model. The liquid film diffusion model is represented by the equation below.

$$\ln(1-Q_t/Q_e) = -k_{fd}t \quad (18)$$

Or

$$\ln(1-F) = -k_{fd}t \quad (19)$$

Table 4. Modeling of adsorption mechanism of cadmium metal ion.

Kinetic models	**Kinetic parameters**	**Numerical values**
Intraparticle diffusion kinetic model	k_{ipd1} (**µ**g $g^{-1}min^{-0.5}$) Intercept R^2	1.11 36.0 0.998
Film diffusion kinetic model	k_{fd} (µg g^{-1} min^{-1}) Intercept R^2	0.047 1.5 0.981

The fractional attainment of equilibrium is denoted by F (Qt /Qe). Kfd is the film diffusion rate constant. Adsorption is thought to occur via the film diffusion process if the graph of ln (1-F) vs t is a straight line with zero intercepts. The film diffusion rate constant, intercept, and regression constant (R2) were 0.047 (µg g-1 min1), 1.5, and 0.981, respectively (Table 4). The straight line passes through the origin with a minor deviation from the zero intercept (-1.5). This deviation from zero may be attributed to the kinetic experiments' high rate of agitation. Furthermore, the small deviation from zero may be explained by a difference in mass transfer rates between the preliminary and final stages of the adsorption process. Comparable findings have been published in the literature [47-49]. The liquid film diffusion mechanism thus regulated Cd(II) adsorption on the adsorbent. The developed method was applied in real water samples and found to be effective.

4. Conclusion

The yield of nanoparticles obtained was 92%. FT-IR, XRD, SEM, and TEM techniques were used to classify the prepared nanoparticles. The surface of the nanoparticles was rough, with iron nanoparticles ranging in size from 10 to 50 nanometers. In batch mode, the formed nanoparticles were used to extract cadmium metal ions from water. With a 25.0 µg/L concentration, 60 minutes contact time, 7.0 pH, 0.5 g/L dose, and a temperature of 25 ºC, the maximum removal of cadmium was 48.2 µg /g. The Langmuir, Freundlich, Temkin, and Dubinin-Radushkevich models all predicted the sorption performance. At 15, 25, and 35 ºC, the thermodynamic parameters ΔG°, ΔH° and ΔS° were -8.0, -9.93, and -12.24, respectively, with -37.79 x 102 kJ/mol and -30.96 x 10-3 kJ/mol K. The endothermic existence of cadmium metal ion removal was verified by these findings. Along with the liquid film diffusion process, the adsorption adopted pseudo-second-order kinetics. The documented adsorption method is fast, environmentally friendly, and inexpensive, and it can be used to test for the removal of cadmium metal ions in natural water samples.

Conflict of interest

The authors declare no conflict of interest.

Acknowledgment

The authors are thankful to the Department of Chemistry, Taibah University, Al-Madinah Al-Munawwarah, Saudi Arabi for providing all necessary facilities.

References

1. Imran, A., Alexandr, E. Burakov, A.V., Melezhik, A.V., Babkin, I.V., Burakova, E.A., Neskomornaya, E.V., Galunin, A.G., Tkachev, D.V. and Kuznetsov, K. Thermodynamics and mechanism of copper and zinc metal ions removal in water on newly synthesized polyhydroquinone/graphene nanocomposite material, ChemSelect, 2019, **4**, 12708-12718.
2. Imran, A., Kon'kova, T., Than, Z., Htay, Hein Thu Aung., Mishenko, E., Mohammad, N.S., Abdulraheem, S.A., Almalki, A., Alhadhrami, A., Alsubaie, A.M., Alharbi, H.A. Economic and fast electro-flotation extraction of heavy metals from wastewater, Environ. Technol., 43, 4019-4028 (2022).
3. Imran, A., Omar, M.L., Alharbi, Z., Alothman, A. and Ahmad, Y.B. Kinetics, thermodynamics and modeling of amido black dye photo-degradation in water using Co/TiO_2 nanoparticles, Photochem. and Photobiol., 2018, **94**, 935-941.
4. Imran, A., Tatiana, S., Kuznetsova, A.E., Burakov, I.V., Burakova, T.V., Pasko, T.P., Dyachkova, E.S., Mkrtchyan, A.V., Babkin, A.G., Tkachev, H.M., Albishri, W.H., Alshitari, A.M.H and Alharbi, A. Polyaniline modified CNTs

and graphene nanocomposite for removal of lead and zinc metal ions: Kinetics, thermodynamics and desorption studies, Molecules, 27, 5623 (2022).
5. Imran, A., Gunel, T., Imanova, H.M., Albishri, W.H., Alshitari, A.M.H., Marcello, L., Mohammad, N.S. and Ahmed, M.H. An ionic-liquid-imprinted nanocomposite adsorbent: simulation, kinetics and thermodynamic studies of triclosan endocrine disturbingwater contaminant removal, Molecules, 7, 5358 (2022).
6. Imran, A., Omar, M.L., Alharbi, Z.A., ALOthman, A.A., Amal, M. Al-Mohaimeed. Preparation of a carboxymethylcellulose-iron composite for the uptake of atorvastatin in water, Int. J. Biol. Macromol. 2019, **132**, 244-253.
7. Nora, H. Al-Shaalan, Imran, A., Zeid, A. ALOthman., Lamya, H. Al-Wahaibi and Hadeel, A. High-performance removal and simulation studies of diuron pesticide in the water on MWCNTs, J. Mol. Liq., 289, 111039 (2019).
8. Imran, A., Neskoromnaya, E.A., Melezhik, A.V., Babkin, A.V., Kulnitskiy, B.A., Burakov, A.E., Burakova, I.V., Tkachev, A.G., Abdulraheem, S.A., Almalki, A. Alsubaie. Magnetically active nanocomposite aerogels: preparation, characterization and application for water treatment, J. Pour. Mat., 2022, **29**, 545-557.
9. Hu, Jun, Donglin Zhao, and Xiangke Wang. Removal of Pb (II) and Cu (II) from aqueous solution using multiwalled carbon nanotubes/iron oxide magnetic composites. Water Sci. Technol. 2006, **63(5)**, 917-923.
10. Srivastava, S.K., Bhattacharjee, G., Tyagi, R., Pant, N. and Pal, N. Studies on the removal of some toxic metal ions from aqueous solutions and industrial waste. Part I (Removal of lead and cadmium by hydrous iron and aluminum oxide). Environ. Technol. 1988, **9(10)**, 1173-1185.
11. Ozay, O., Ekici, O., Baran, Y., Aktas, N. and Sahiner, N. Removal of toxic metal ions with magnetic hydrogels. Water Res. 2009, **43(17)**, 4403-4411.
12. Jamil, M., Muhammad S.Z. and Muhammad, Q. Contamination of agro-ecosystem and human health hazards from wastewater used for irrigation. J. Chem. Soc. Pak. 2010, **32(3)**, 370-378.
13. Khan, S., Cao, Q., Zheng, Y.M., Huang, Y.Z. and Zhu, Y.G. Health risks of heavy metals in contaminated soils and food crops irrigated with wastewater in Beijing, China. Environ. Pollut. 2008, **152(3)**, 686-692.
14. Singh, A., Sharma, R.K., Agrawal, M. and Marshall, F.M. Health risk assessment of heavy metals via dietary intake of foodstuffs from the wastewater irrigated site of a dry tropical area of India. Food Chem. Toxicol. 2010, **48(2**), 611-619.
15. Peng, S.-H., Wang, W.-X., Li, X. and Yen, Y.-F. Metal partitioning in river sediments measured by sequential extraction and biomimetic approaches. Chemosphere. 2004, **57(8)**, 839-851.
16. Kuppusamy, P., Yusoff, M.M., Maniam, G.P. and Govindan, N. (2016). Biosynthesis of metallic nanoparticles using plant derivatives and their new avenues in pharmacological applications-An updated report. Saudi Pharm J. 2016, **24(4)**, 473-484.
17. Zhang, Wei-xian. Nanoscale iron particles for environmental remediation: an overview. J Nanopart Res. 2003, **5(3)**, 323-332.
18. Deliyanni, E.A. and Matis, K.A. Sorption of Cd ions onto akaganeite-type nanocrystals. Sep. Purif. Technol. 2005, **45(2)**, 96-102.
19. Niu, S.-f., Liu, Y., Xin-hua, Xu, X.-h. and Lou, Z.H. Removal of hexavalent chromium from aqueous solution by iron nanoparticles. *Journal of Zhejiang University-Science B.* 2005, **6(10)**, 1022-1027.
20. Lazaridis, N.K., Bakoyannakis, D.N. and Deliyanni, E.A. Chromium (VI) sorptive removal from aqueous solutions by nanocrystalline akaganeite. Chemosphere. 2005, **58(1)**, 65-73.
21. Hu, J., Guohua, C. and Irene, MC, Lo. Removal and recovery of Cr (VI) from wastewater by maghemite nanoparticles. Water Res. 2005, **39(18)**, 4528-4536.
22. Di, Z.C., Ding, J., Peng, X.J., Li, Y.H., Luan, Z.K. and Liang, J. Chromium adsorption by aligned carbon nanotubes supported ceria nanoparticles. Chemosphere. 2006, **62(5)**, 861-865.
23. Bing, G., Zhaohui, J., Tielong, L. and Xinhua, Q. Kinetics of hexavalent chromium removal from water by chitosan-Fe0 nanoparticles. Chemosphere. 2009, **75(6**), 825-830.
24. Agarwal, H., Venkat, K.S. and Rajeshkumar, S. A review on green synthesis of zinc oxide nanoparticles–An eco-friendly approach. Resource-Efficient Technologies. 2017, **3(4)**, 406-413.
25. Mohammadlou, M., Maghsoudi, H. and Jafarizadeh-Malmiri, H. A review on green silver nanoparticles based on plants: Synthesis, potential applications and eco-friendly approach. *International Food Research Journal*. 2016; **23(2)**.
26. Imran, A., Mohd, S., Eva, C., López, R., Khattab, A., Hassan, M. and Albishri, W.H. Advances in graphene-based materials for the treatment of water, *Arabian Journal of Geosciences*. 15, 521(2022).
27. Ehrampoush, M.H., Miria, M., Salmani, M.H. and Mahvi, A.H. Cadmium removal from aqueous solution by green synthesis iron oxide nanoparticles with tangerine peel extract. *Journal of Environmental Health Science and Engineering*. 2015, **13(1)**, 1-7.
28. Abdullah, J.A.A., Eddine, L.S., Abderrhmane, B., Alonso-González, M., Guerrero, A. and Romero, A. Green synthesis and characterization of iron oxide nanoparticles by pheonix dactylifera leaf extract and evaluation of their antioxidant activity. *Sustain.* Chem. Pharm**.** 2020, **17**, 100280.
29. Laid, T.M., Abdelhamid, K., Eddine, L.S. and Abderrhmane, B. Optimizing the biosynthesis parameters of iron oxide nanoparticles using central composite design. *Journal of Molecular Structure*. 2021, 1229, 129497.

30. Ehrampoush, M.H., Miria, M., Salmani, M.H. and Mahvi, A.H. Cadmium removal from aqueous solution by green synthesis iron oxide nanoparticles with tangerine peel extract. *Journal of Environmental Health Science and Engineering*, 2015, **13(1)**, 1-7.
31. Zhu, F., Ma, S., Liu, T. and Deng, X. Green synthesis of nano zero-valent iron/Cu by green tea to remove hexavalent chromium from groundwater. J. Clean. 2018, **174**, 184-190.
32. Imran, A., Tatiana, K., Elena, L., Ekaterina, S., Zeid, A., ALOthman, A., Taghrid, S., Alomar, M. and Ataul, I. Preparation and characterization of SnO_2-CeO_2 nanocomposites: Sorption, modeling and kinetics for azorubine dye removal in water, *Journal of Molecular Liquid*. 346, 117119 (2022).
33. Zeid, A., ALOthman, A., AlMasoud, N., Mbianda, X.Y. and Imran A. Synthesis and characterization of γ-cyclodextrin-graphene oxide nanocomposite: Sorption, kinetics, thermodynamics and simulation studies of tetracycline and chlortetracycline antibiotics removal in water, *Journal of Molecular Liquid*. 345, 116993 (2022).
34. Imran, A., Zakharchenko, E.A., Myasoedova, G.V., Molochnikova, N.P., Rodionova, A.A., Baulin, V.E., Burakov, A.E., Burakova, I.V., Babkin, A.V., Neskoromnaya, E.A., Melezhik, A.V., Tkachev, A.G., Mohamed A.H., Adel El-Marghany, M.S. and Ayman, G. Preparation and characterization of oxidized graphene for actinides and rare earth elements removal in nitric acid solutions from nuclear wastes, *Journal of Molecular Liquid*., 335, 116260 (2021).
35. Imran, A., Tatiana, K., Vitalii, K., Anton, R., Stefan, P., Mbianda. X.Y., Mohamed, A.H. and AlMasoud, N. Preparation and characterization of nano-structured modified montmorillonite for dioxidine antibacterial drug removal in water, *Journal of Molecular Liquid*. 331, 115770 (2021).
36. Imran, A., Alexander, V., Babkin, I.V., Burakova, A.E., Burakov, E.A., Neskoromnaya, A.G., Tkachev, S.P., AlMasoud, N., Taghrid, S. Alomar. Fast removal of samarium ions in water on highly efficient nanocomposite-based graphene oxide modified with polyhydroquinone: Isotherms, kinetics, thermodynamics and desorption, J. Mol. Liq., 329, 115584 (2021).
37. Zeid, A., ALOthman, A., Yacine, B., Osamah, M., Alduhaish, K., Rathinam, S.P. and Imran, A. Synthesis, characterization, kinetics and modeling studies of new generation pollutant ketoprofen removal in water using copper nanoparticles, *Journal of Molecular Liquid*. 323, 115075 (2021).
38. Zeid, A., ALOthman, Ahmad., Yacine, Badjah., Omar, M.L., Alharbi. and Imran, A. Copper carboxymethyl cellulose nanoparticles for efficient removal of tetracycline antibiotics in water, *Environmental Science and Pollution Research*. 2020, **27**, 42960-42968.
39. Imran, A., Shirin, A., Yousef, P., Ali, A., Yousef, R., Abolfazl, F., Asghar, H. and Mehdi, F. Green preparation of activated carbon from pomegranate peel coated with zero-valent iron nanoparticles (nZVI) and isotherm and kinetic studies of amoxicillin removal in water, *Environmental Science and Pollution Research*. 2020, **27**, 36732-36743.
40. Panwar, V., Kumar, P., Bansal, A., Ray, S.S. and Jain, S. Gylated magnetic nanoparticles (PEG@ Fe_3O_4) as cost effective alternative for oxidative cyanation of tertiary amines via CH activation. Applied Catalysis A: General. 2015, **498**, 25-31.
41. Langmuir, Irving. The adsorption of gases on plane surfaces of glass, mica and platinum. *Journal of American Chemical Society*. 1918, **40(9)**, 1361-1403.
42. Temkin, M.I. Kinetics of ammonia synthesis on promoted iron catalysts. Acta Physiochim. URSS. 1940, **12**, 327-356.
43. Dabrowski, A. Adsorption-from theory to practice, Adv. Colloid Interface. Sci. 2001, **93**, 135-224.
44. Hobson, John P. Physical adsorption isotherms extending from ultrahigh vacuum to vapor pressure. *Journal of Physical Chemistry*. C. 1969, **73(8)**, 2720-2727.
45. Chien, S.H. and W.R. Clayton. Application of Elovich equation to the kinetics of phosphate release and sorption in soils 1. *Soil Science Society of American Journal*. 1980, **44(2)**, 265-268.
46. Boyd, G.E., Adamson, A.W. and Myers, L.S. The Exchange Adsorption of Ions from Aqueous Solutions by Organic Zeolites. II. Kinetics, *Journal of American Chemical Society*. 1947, **69**, 2836-2848.
47. Zeid, A., ALOthman, A., Yacine, B., Omar, M.L. Alharbi. and Imran, A. Synthesis of chitosan composite iron nanoparticles for removal of diclofenac sodium drug residue in water, International Journal of Biological Sciences. Macromol., 2020, **159**, 870-876.
48. Imran, A., Omar, M.L. Alharbi., Zeid, A., ALOthman, A., Amal, Mohammed., Al-Mohaimeed., Abdulrahman, Alwarthan. Modeling of fenuron pesticide adsorption on CNTs for mechanistic insight and removal in water, Environ. Res., 2019, **170**, 389-397.
49. Zeid, A., ALOthman, A., Yacine, B. and Imran, A. Facile synthesis and characterization of multi-walled carbon nanotubes for fast and effective removal of 4-tert-octylphenol endocrine disruptor in water, *Journal of Molecular Liquid*. 2019, **275**, 41-48.

Received 25 May 2023
Accepted 25 June 2023